MAIN LANDING GEAR DOORS VIBRATION REDUCTION BASED ON FLIGHT TEST ICAS2020 1049

R. Abarca[1], C. Aquilini[2], P. Lubrina[3], S.–H. Peng[4], J. Schwochow[5]

[1]AIRBUS Operations S.L. Getafe, Madrid, Spain
[2]AIRBUS Defense and Space. Manching, Germany
[3]ONERA, The French Aerospace Lab, Châtillon, France
[4]FOI, Swedish Defence Research Agency, Stockholm, Sweden
[5]DLR, German Aerospace Center, Göttingen, Germany

ICAS2020_1049

AFLONext
2ND GENERATION ACTIVE WING

32nd Congress of the International Council of the Aeronautical Sciences
September 6-10, 2021
Pudong Shangri-La, Shanghai, China

INDEX

- Introduction
- The Computational Aerodynamic Analysis
- The Ground Vibration Test
- Update of the Finite Element Model
- CFD-CSM Coupling: The Buffeting Analysis
- Control Means for Structural Response Reduction
- Flight Test Results
- Conclusions

Introduction

- **Main landing gear doors** cover the main landing gear bays, keeping the aerodynamic shape of the aircraft during flight.
- They are open/close on each landing gear retraction/extension.
- During these phases, the nose landing gear creates **flow separations**, characterized by turbulent vortex motions.
- This turbulent flow is responsible of **unsteady aerodynamic loads** on the main landing gear doors and may lead to vibrations (buffeting).
- The present work summarizes the key activities carried out to characterize the **structural response** of the main landing gear doors of a commercial transport aircraft.
- **Control devices** designed, manufactured and flight-tested in order to mitigate their vibrations.

Computational Aerodynamic Analysis

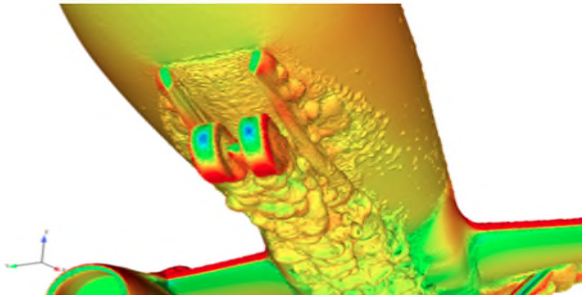

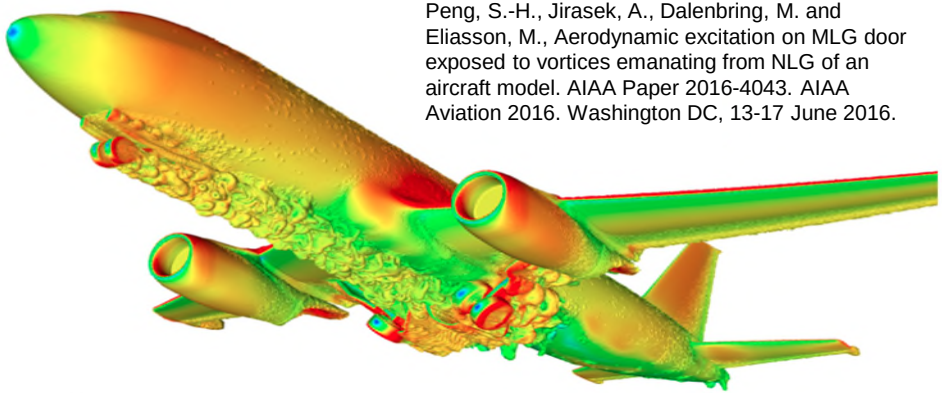

Peng, S.-H., Jirasek, A., Dalenbring, M. and Eliasson, M., Aerodynamic excitation on MLG door exposed to vortices emanating from NLG of an aircraft model. AIAA Paper 2016-4043. AIAA Aviation 2016. Washington DC, 13-17 June 2016.

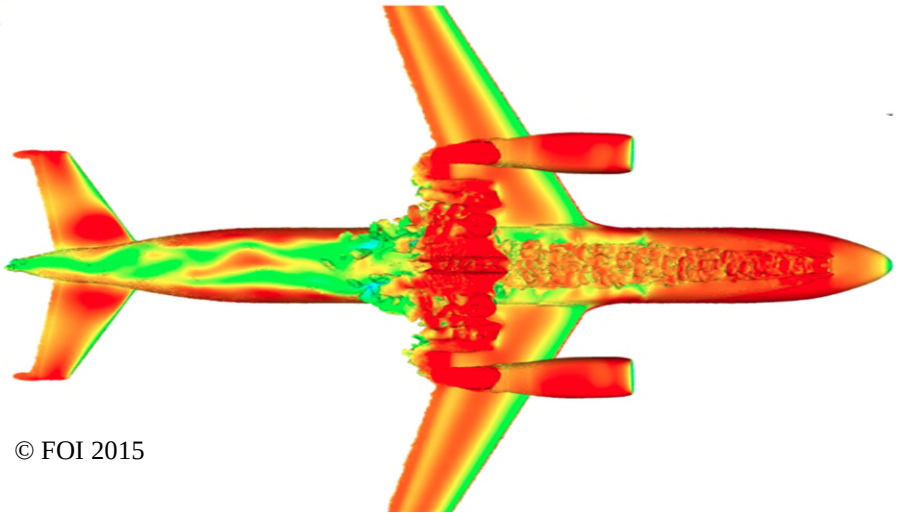

Vorticity iso-surface contoured by velocity.Isometric view

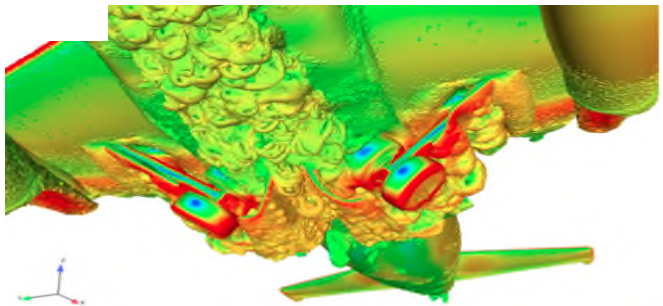

Computational Aerodynamic Analysis (cont'd)

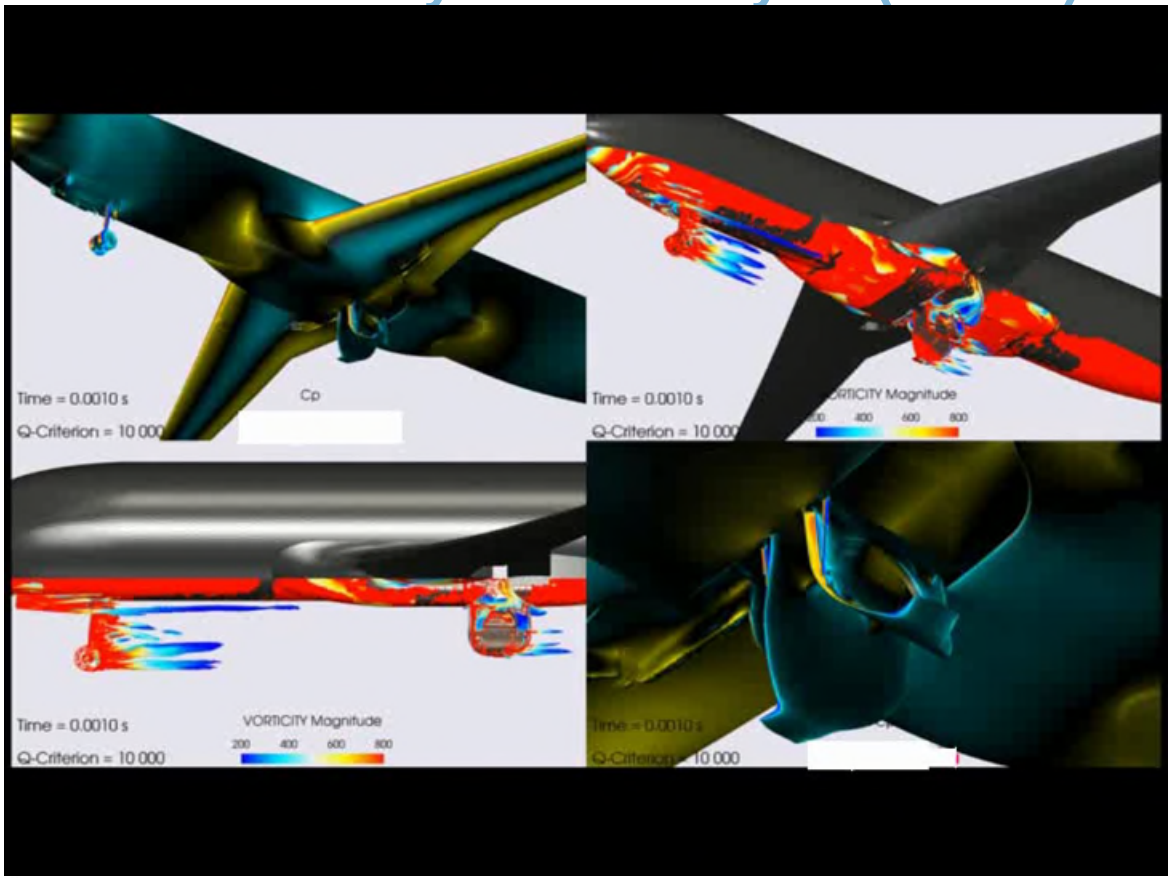

Tomac, M., A. Rizzi, D. Charbonnier, J.B. Vos, A. Jirasek, S-H. Peng, A. Winkler, A. Allen, G. Wissocq, G. Puigt, J. Dandois, R. Abarca. Unsteady Aero-Loads from Vortices Shed on A320 Landing Gear Door: CFD compared to fight tests. . AIAA Paper 2016-0803.

The Ground Vibration Test

- A Ground Vibration Test was performed on the **left MLGD** of the transport aircraft **DLR ATRA**.
- The right hand side MLG door was closed.
- The A/C was on ground on **inflated tires**. Fuel empty.
- The **hydraulic system** was **active** and the control surfaces were in neutral position.
- **Three** different values for the **MLGD actuator pressure** (nominal, medium and zero) were tested.

The Test Setup

The FEA Model of the isolated MLGD guided the selection of the locations for the sensors and excitations.

- A total of **90 accelerometers** were attached on the MLGD, actuator fittings, door hinges and on the rest of the A/C. One accelerometer was used for cycle monitoring.
- **1 Strain gauge** was installed and conditioned on the actuator;
- As **force measurement**, force cells and the force current in the shaker coil were used.
- A **bungee cord** was installed between the door and a fixed placed in the test hall in order to remove the MLGD free play.

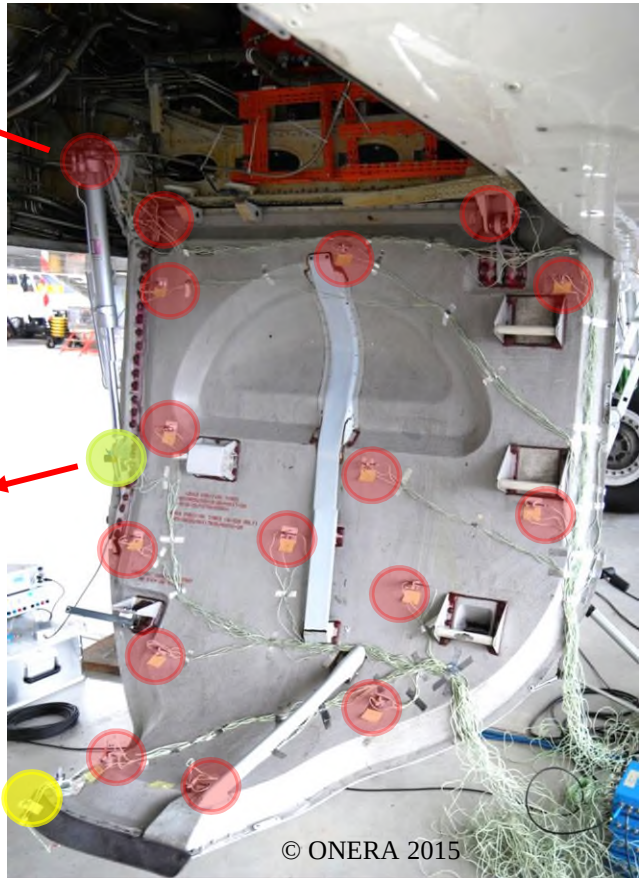

The Test Setup (cont'd)

Four excitation locations and directions:

1. **Y A/C axis**: adapter glued on the outer surface of the door;
2. **X A/C axis**: adapter screwed at the door tip;
3. **Z A/C axis**: same as 2.
4. **2nd Y A/C axis**: adapter glued on the outer surface of the door.

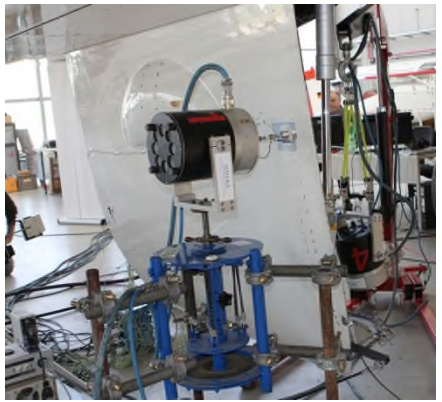

1. 1st Lateral Excitation

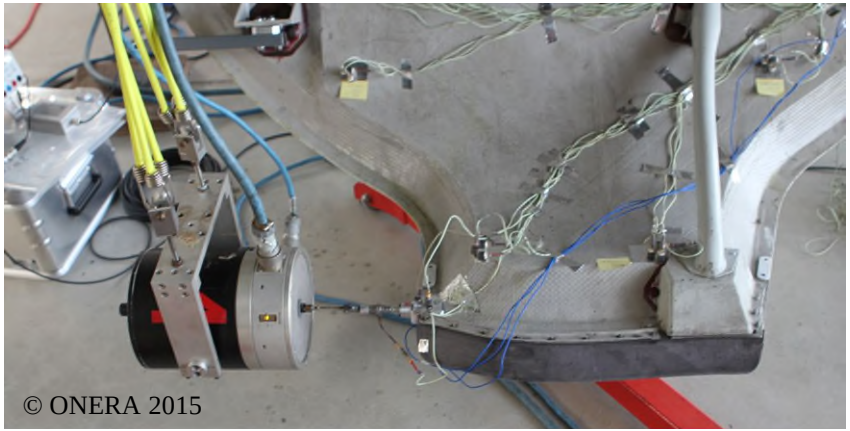

2. Bottom Axial Excitation

3. Bottom Vertical Excitation

4. 2nd Lateral Excitation

Examples

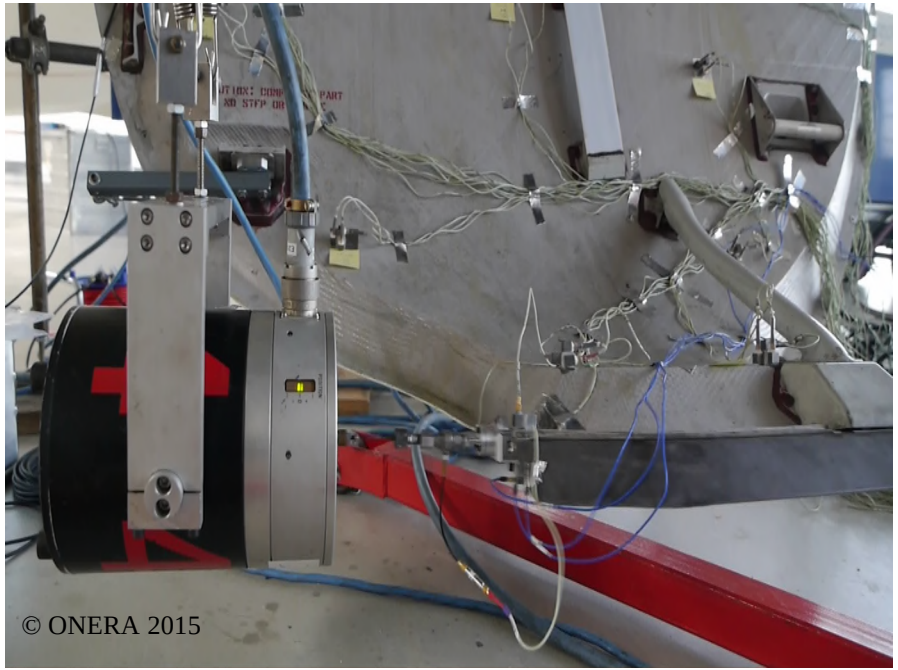

Bottom axial excitation of the second mode with stroboscopic effect due to the proximity of the resonance frequency with one subharmonic of high-speed camera.

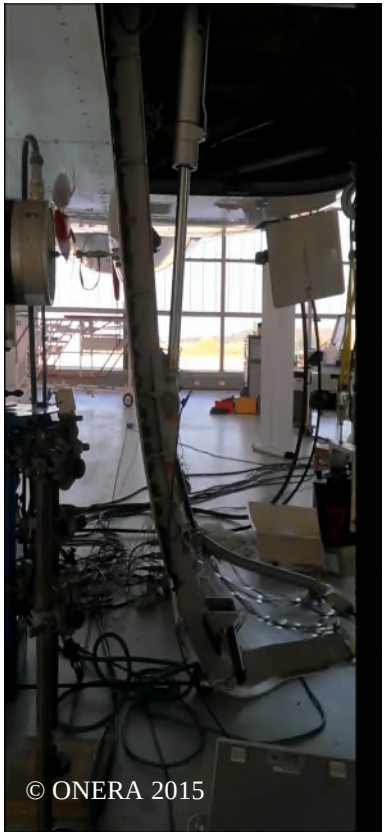

Lateral Excitation

The Acquisition System, Software and Test Methods

- **Acquisition system:**
  - **LMS Scadas III** using
    - V12L conditioning and Analogic-Digital 24 bits converters;
    - QDAC 2 (Quad Digital to Analog Converter) signals generator module.
- **Software:**
  - **LMS TestLab MIMO** (Multi Inputs Multi Outputs) workbook for swept sine runs + **ONERA GVT-Tool** software to design the excitation signals and to post-process the measurements in time domain;
  - **LMS TestLab PolyMAX** for the modal parameter extraction in the Phase Separation Method;
  - **LMS TestLab Normal Mode Testing** in the Phase Resonance Method + **ONERA GVT-Tool** software to post-process the measurements.
- **Test Methods:**
  - **PSM (Phase Separation Method)** using swept sines, different levels of forces, time data recording, FRF computation and modal parameters extraction through LMS PolyMAX.
  - **PRM (Phase Resonance Method)** applied separately on target modes with real time controlling of the harmonic excitation tuned at the resonance frequency. Use of the **Force in Quadrature** method for the estimation of the damping coefficient and the generalized mass.

The Modal Shapes (PRM)

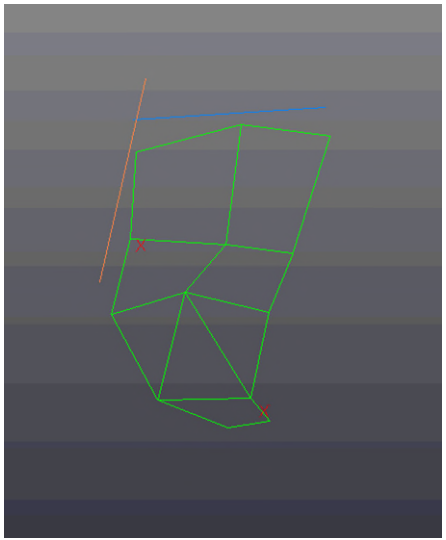

1. Door Rotation

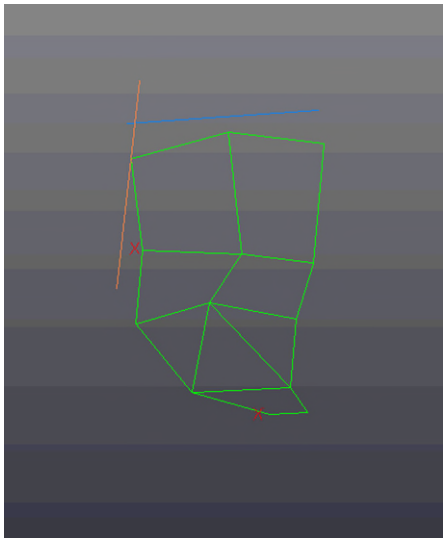

2. 1st Door Torsion

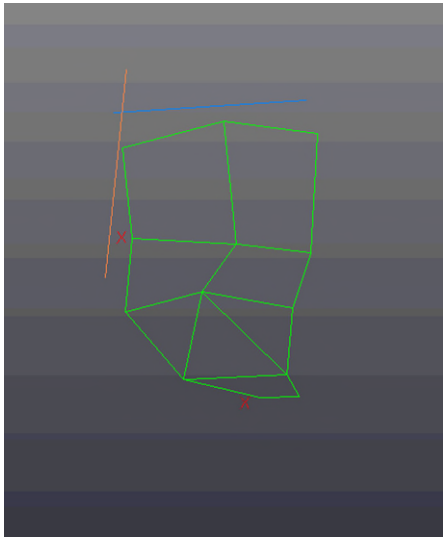

3. 1st Door Bending

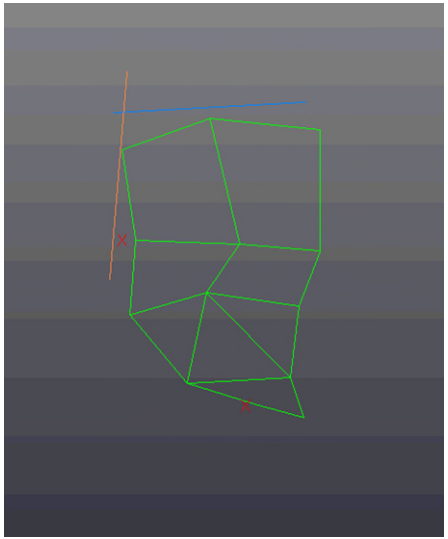

4. 2nd Door Bending

Qualification of the Modes and the Nonlinearity Plots

- The **Modal Assurance Criterion (MAC)** is used to pair, as far as possible, the mode shapes between two mode families or inside a single family. In this case, the AutoMAC label is used.

$$MAC_{n,m} = \frac{\emptyset_n{}^T \times \emptyset_m}{|\emptyset_n|^2 \times |\emptyset_m|^2}$$

- The **Modal Indicator Function (Mif)** quantifies the “purity” of the mode shapes and it is defined as

$$Mif_n = 1 - \frac{\sum(|imag(\emptyset_n)| \times |\emptyset_n|)}{\sum|\emptyset_n|^2}$$

- **Nonlinearities** were investigated for selected modes during the testing with the PRM. The same studies were performed with three different actuator pressures.

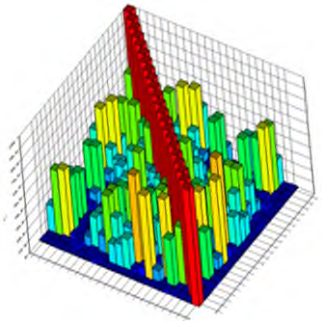

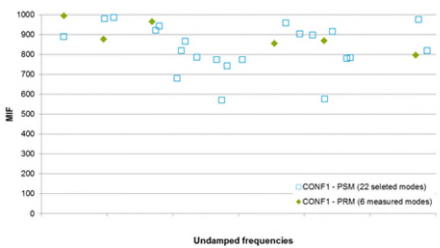

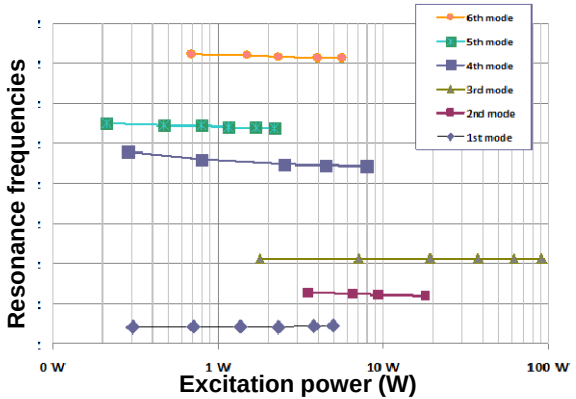

Update of the Finite Element Model

- The GVT highlighted **discrepancies** between the tested MLGD from the original FEM.
- The root cause was identified in some **additional aircraft stiffness**, which participates on the front attachment of the MLGD. This could not be considered in the analytic model of the isolated door.

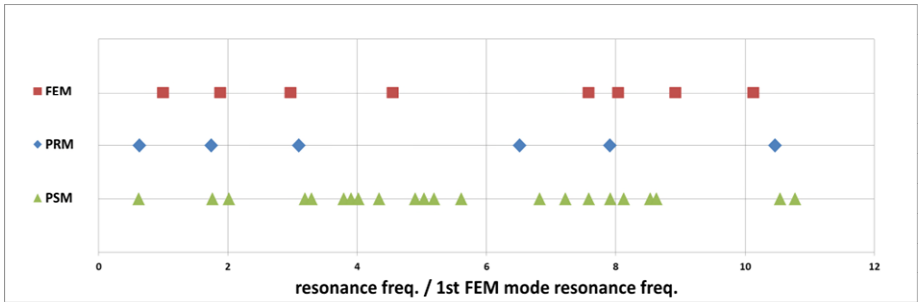

Comparison of FEM and GVT eigenfrequencies, before the model update.

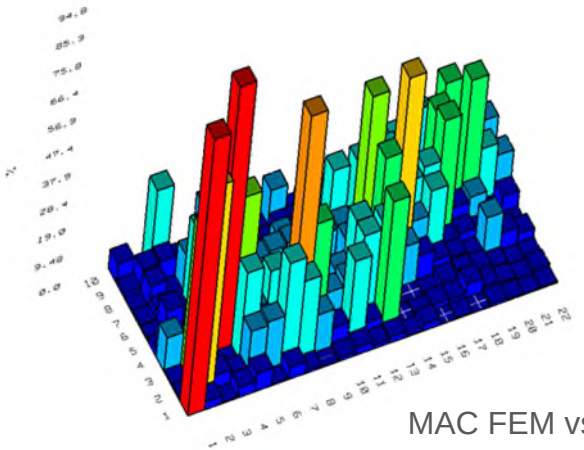

MAC FEM vs. PSM

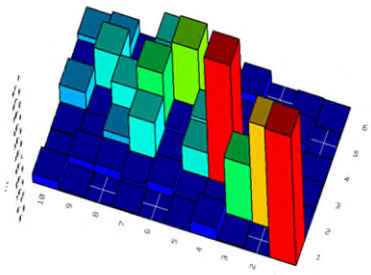

MAC FEM vs. PRM

Update of the Finite Element Model (cont'd)

- As a consequence, the **FEM model required to be updated** in order match the GVT results. The target was to match only the first three elastic modes of the door, which were thought to be the most relevant of the door structural dynamics during in flight.
- Anyway, after the model update, the MAC of the **third mode** continued to show **a non-reliable matching**.

	Updated FEM (f/fref)	GVT (f/fref)	MAC
1st Mode	1.00	0.99	95.2 %
2nd Mode	2.87	2.75	80.6 %
3rd Mode	4.89	4.90	65.6 %

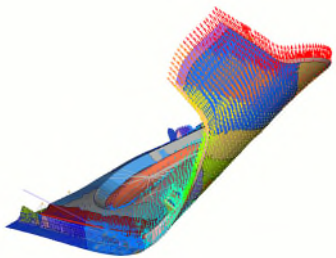

Mode 1

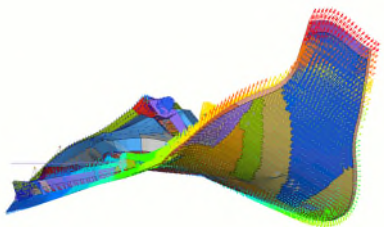

Mode 2

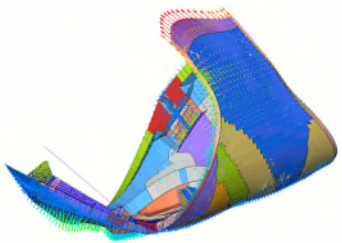

Mode 3

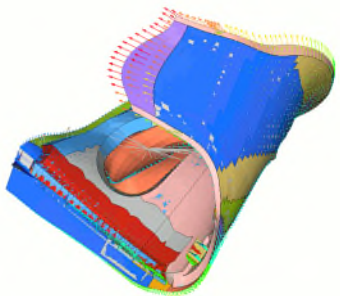

Mode 4

The Buffeting Analysis

Aquilini, C. and Parisse, D. (2017). A Method for Predicting Multivariate Random Loads and a Discrete Approximation of the Multidimensional Design Load Envelope. Como: IFASD 2017

- The aeroelastic response of the structure to the unsteady flow excitation (namely buffeting) was computed in modal space using a stochastic approach, derived for **wide-sense stationary stochastic processes**. The starting point is the availability of the unsteady, motion-independent pressure distribution on a three-dimensional aerodynamic grid (either from CFD or from test measurements) and a structural model.
- The spectrum of the **aerodynamic pressure distribution $\mathbf{S}_{p_k}(j\omega)$ is integrated** obtaining a force distribution $\mathbf{S}_{f_k}(j\omega)$ statically equivalent on the same grid (the aerodynamic grid k).

$$\mathbf{S}_{f_k}(j\omega) = \mathbf{A}_n \mathbf{S}_{p_k}(j\omega)\mathbf{A}_n^{\intercal}$$

- **Surface splines $\mathbf{G}_{kg}$** are then used in order **to interpolate the spectrum of the force distribution**, obtaining an equivalent system on the structural grid g.

$$\mathbf{S}_{f_g}(j\omega) = \mathbf{G}_{kg}^{\intercal}\mathbf{S}_{f_k}(j\omega)\mathbf{G}_{kg}$$

- The **aeroelastic response** of the structure to the unsteady flow excitation (namely **buffeting**) is computed in modal space using a stochastic approach. Considering the transfer function $\mathbf{H}(j\omega) = \left[-\omega^2\widetilde{\mathbf{M}} + j\omega\widetilde{\mathbf{B}} + (1+jg)\widetilde{\mathbf{K}} - q_\infty\widetilde{\mathbf{Q}}(Ma,k)\right]^{-1}$ and the modal matrix $\mathbf{\Phi}$

$$\mathbf{S}_\xi(j\omega) = \mathbf{H}(j\omega)\mathbf{\Phi}^{\intercal}\mathbf{S}_{f_g}(j\omega)\mathbf{\Phi}\mathbf{H}(j\omega)^{\dagger} \quad \Rightarrow \quad \mathbf{S}_u(j\omega), \mathbf{S}_{\dot{u}}(j\omega), \mathbf{S}_{\ddot{u}}(j\omega), \mathbf{S}_Y(j\omega)$$

The Pressure Distribution

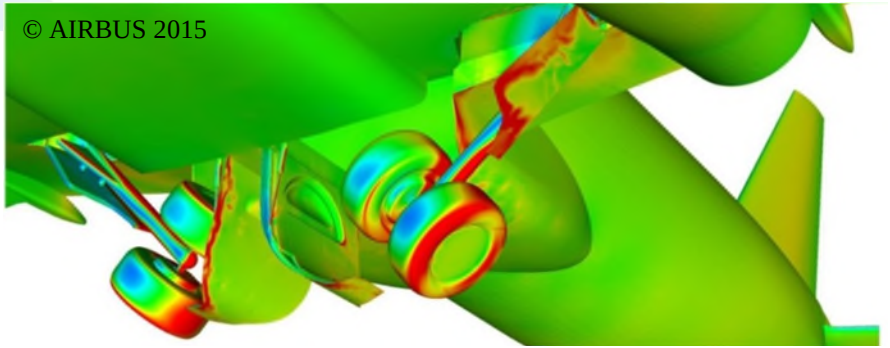

- The door was shaped with **six panels** and a regular three-dimensional grid was generated (**aerodynamic grid**, created by using a parametric bilinear surface, the hyperbolic paraboloid).
- The **pressures were interpolated** over the aerodynamic grid.
- **Auto- and cross-spectra** of the difference between the pressures on the outer and inner surfaces of the door were computed.
- The spectrum of the **pressures** was **integrated** obtaining a statically equivalent force distribution on the aerodynamic grid.
- **Surface splines** were then used to interpolate the spectrum of the aerodynamic forces on the structural grid.

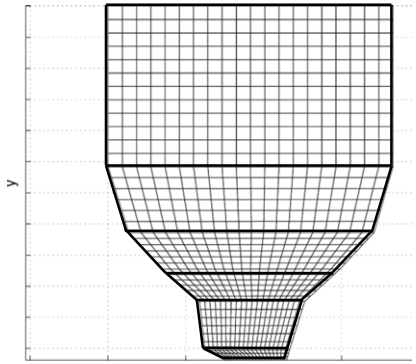

Aerodynamic grid.

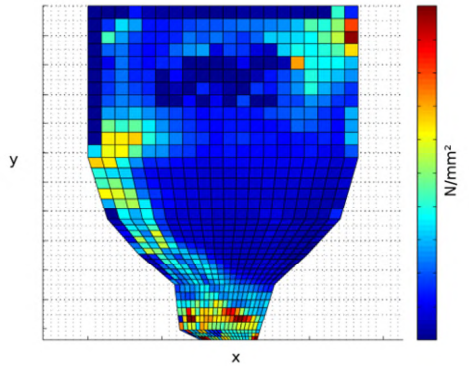

RMS of the interpolated pressures.

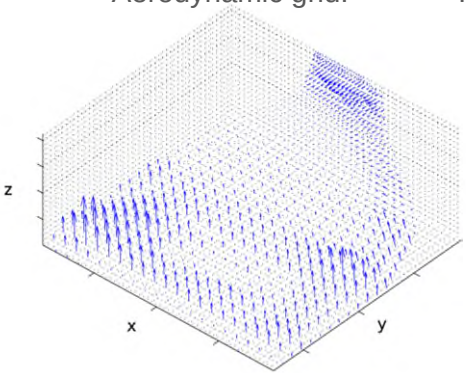

RMS of the forces on the aerodynamic grid.

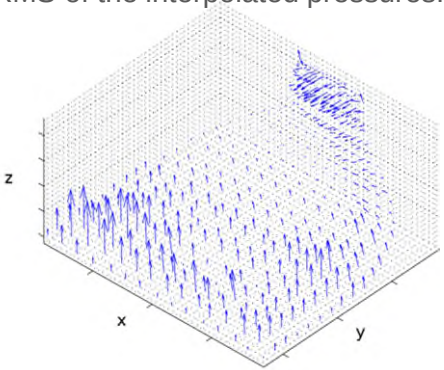

RMS of the forces on the structural grid.

The Stochastic Analysis

- The **buffeting analysis** was finally performed, computing **displacements** and **accelerations** at at four nodes of the door as well as the **reaction forces** at the actuator fitting in terms of auto- and cross-spectra.
- The results of the stochastic analyses are illustrated (red curve) together with measurements (blue curve) in terms of power spectral densities of the actuator loads and accelerations, respectively.

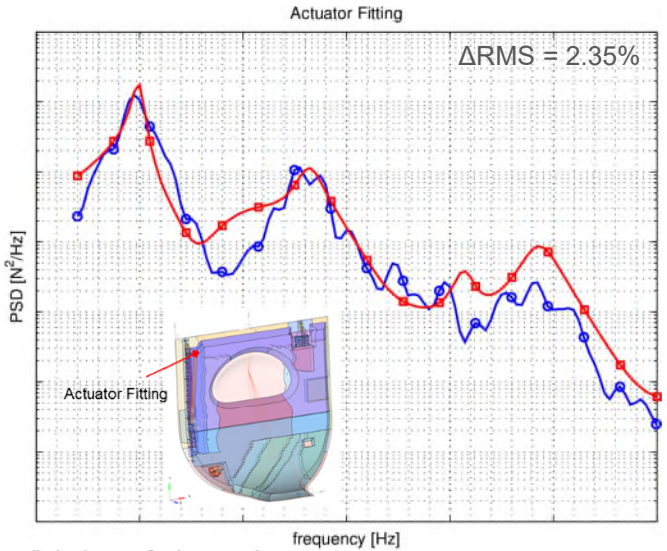

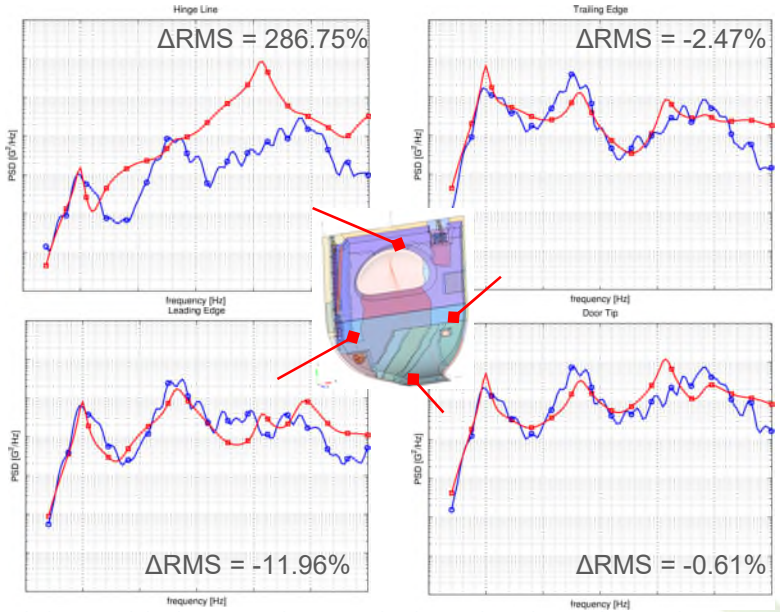

The Stochastic Analysis (cont'd)

- The **buffeting analysis** was finally performed, computing **displacements** and **accelerations** at at four nodes of the door as well as the **reaction forces** at the actuator fitting in terms of auto- and cross-spectra.
- The results of the stochastic analyses are illustrated (red curve) together with measurements (blue curve) in terms of power spectral densities of the actuator loads and accelerations, respectively.
- **Excluding the third mode** from the modal base and repeating the buffeting analysis sensibly improves the results at the hinge line location.

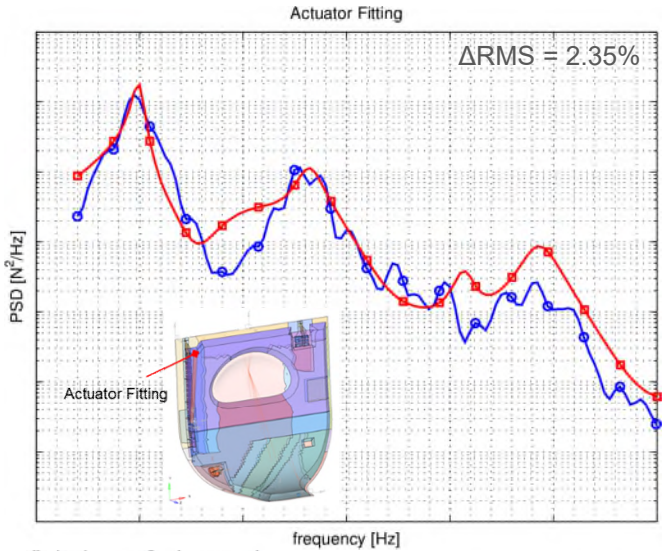

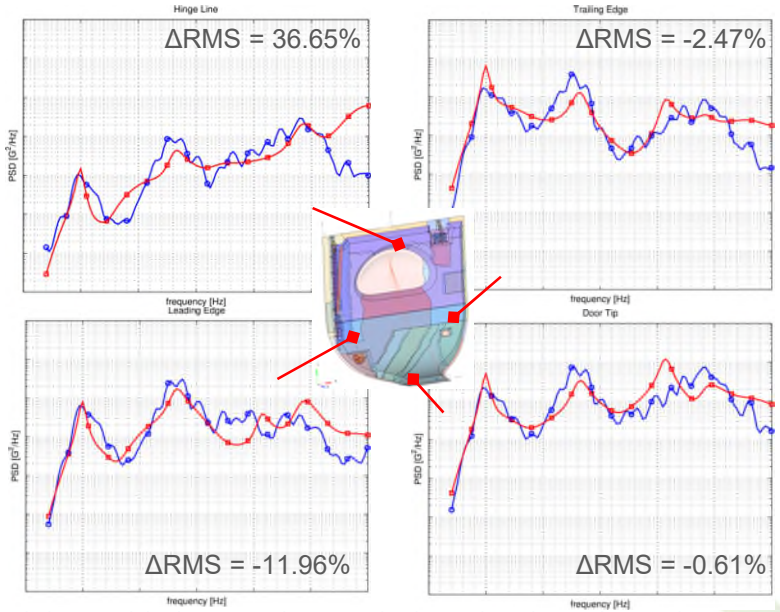

Control Means: Vortex Generators

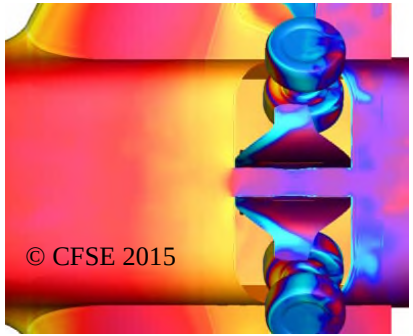

Observation: From unsteady CFD, strong vortex is identified from door outer face that influences door pressure RMS → may lead to increase structural response.

Design Objective: Apply flow control to reduce this vortex by array of vortex generators installed on outer door face.

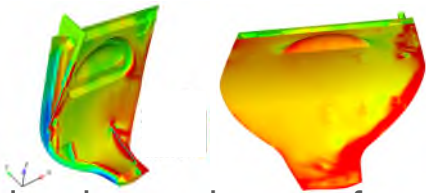

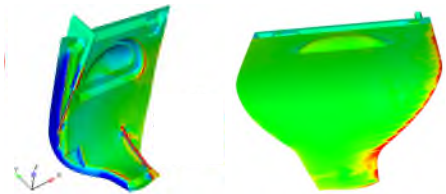

Theoretical benefit: Reduced delta Pressure RMS levels on door surface with VG installed → Structural 1st bending door mode expected high reduction on lateral displacements.

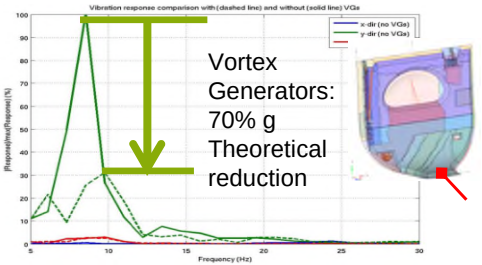

Prototype:

Control Means: Deflectors

Observation: Door local angle of attack is changing every 50 ms from one door side to the opposite → Door oscillating forces being generated.

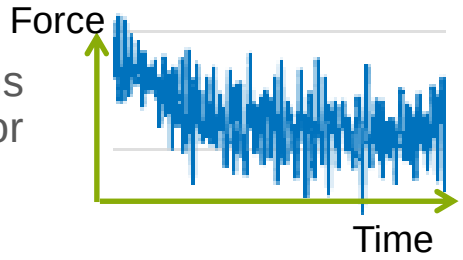

Design Objective: Modify door leading edge with flat inclined plate in front of incoming airflow.

Theoretical benefit: Create less sensible door leading edge to continuous sudden variations of door angle of attack.

Drawback: Dynamic pressure dependent.

Prototype: 4 blocks along door inner face on leading edge considering design compatibility with door operation / structure.

Control Means: Spoiler

Observation: When landing gear passing near the open doors there is a net open door tendency that influence the structural response.

Design Objective: Install a spoiler to generate closing door tendency.

Theoretical benefit: More balanced aerodynamic load should reduce the structural preload and provide less structural response.

Drawback: Highly speed dependency being a lifting surface.

Prototype:

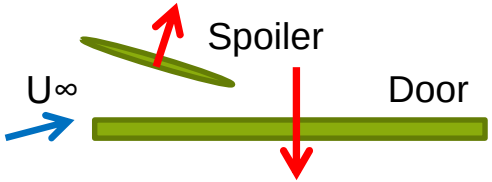

Flight-tested Devices

Three different devices have been flight-tested:

- 1 reference flight with no device installed.
- 1 flight with Vortex Generators on LH and RH doors.
- 1 flight with:
  Deflectors on LH door
  Spoiler on RH door

Vortex Generators

Leading Edge Deflectors

Leading Edge Spoiler

Flight Test Installation

- Strain gauge
- Unsteady pressure sensors
- Accelerometers
- Landing Gear and door positions
- External camera

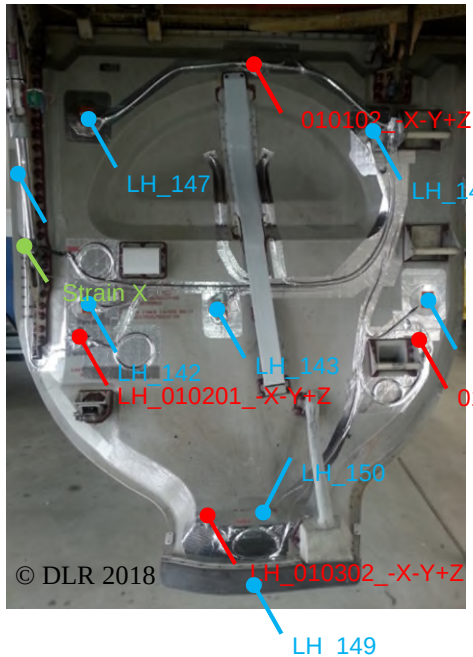

Flight Test Results

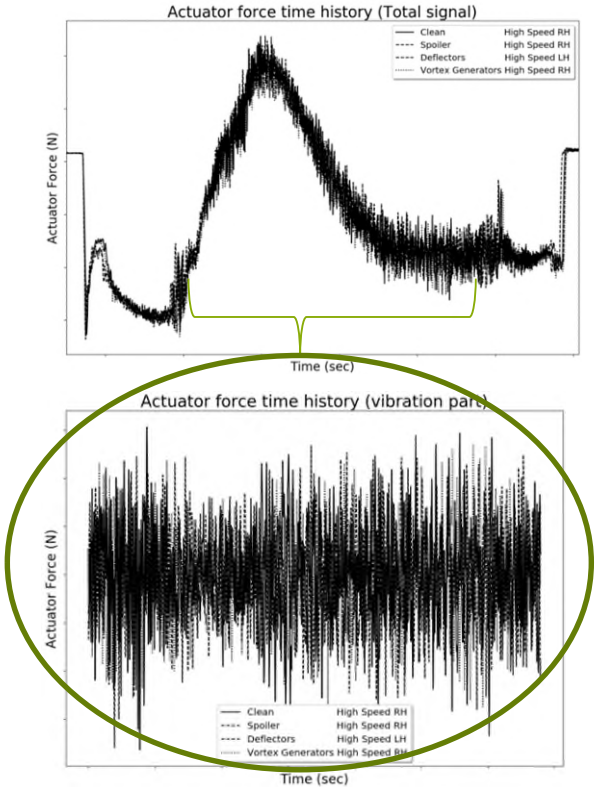

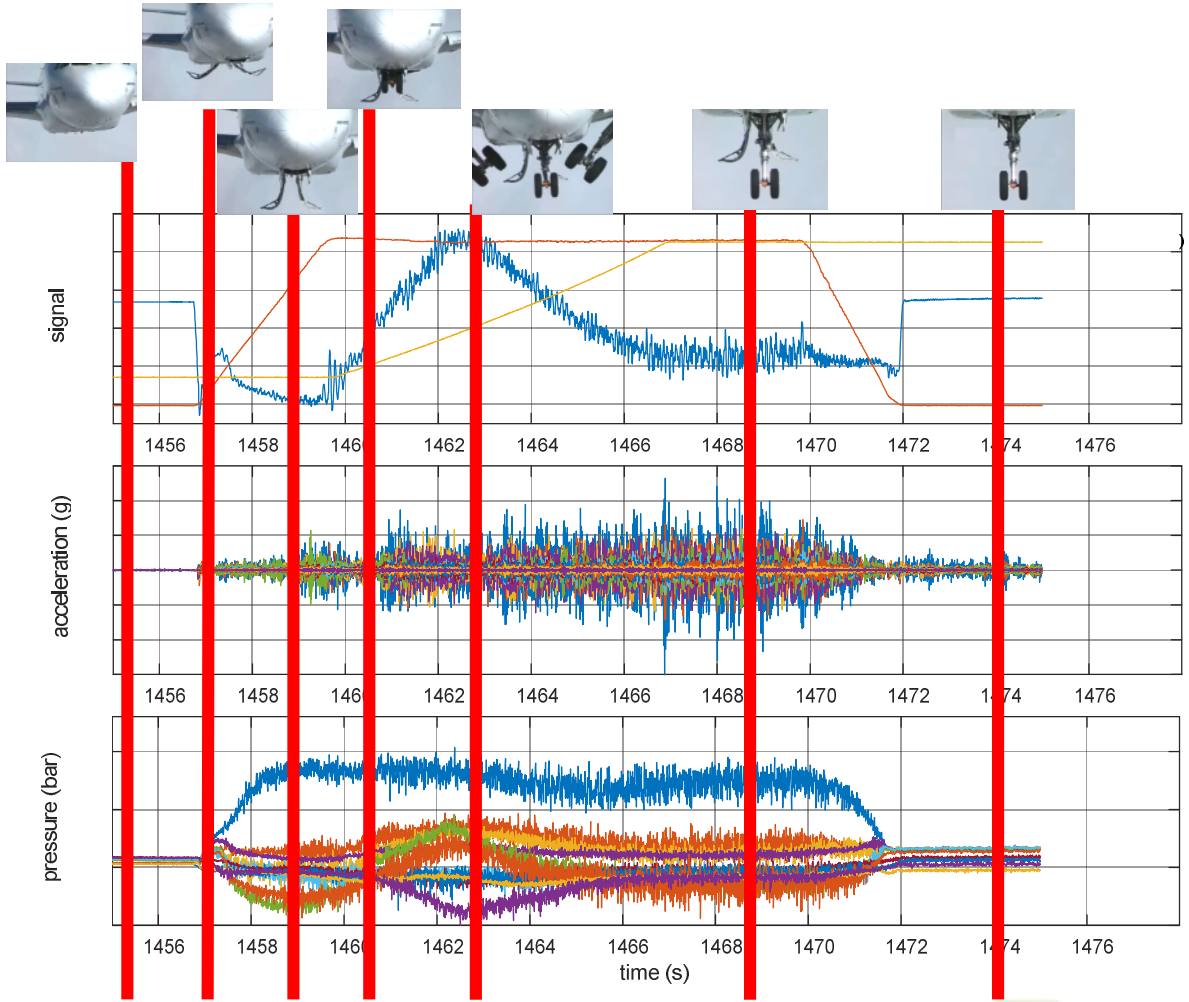

Actuator Door Force RMS Comparison

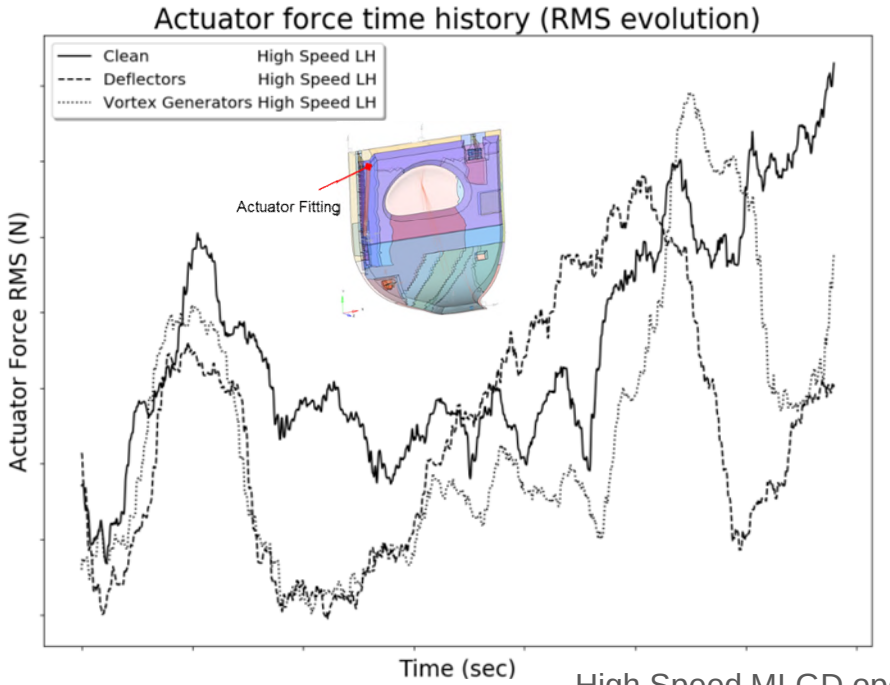

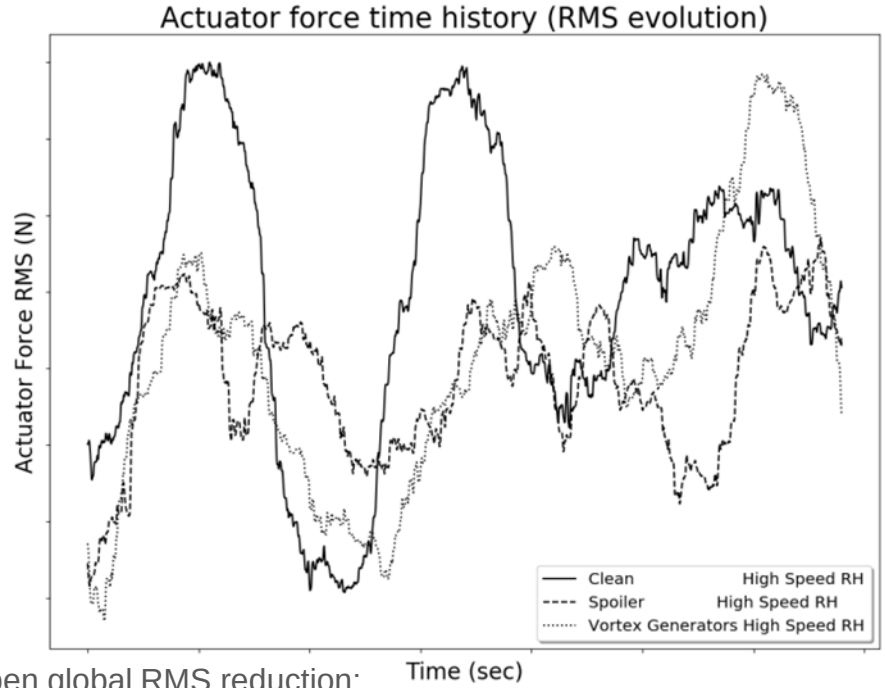

High Speed MLGD open global RMS reduction:
Vortex Generators = 10.6%
Deflectors = 12.5%
Spoiler = 11.2%

Actuator Door Force RMS Comparison (cont'd)

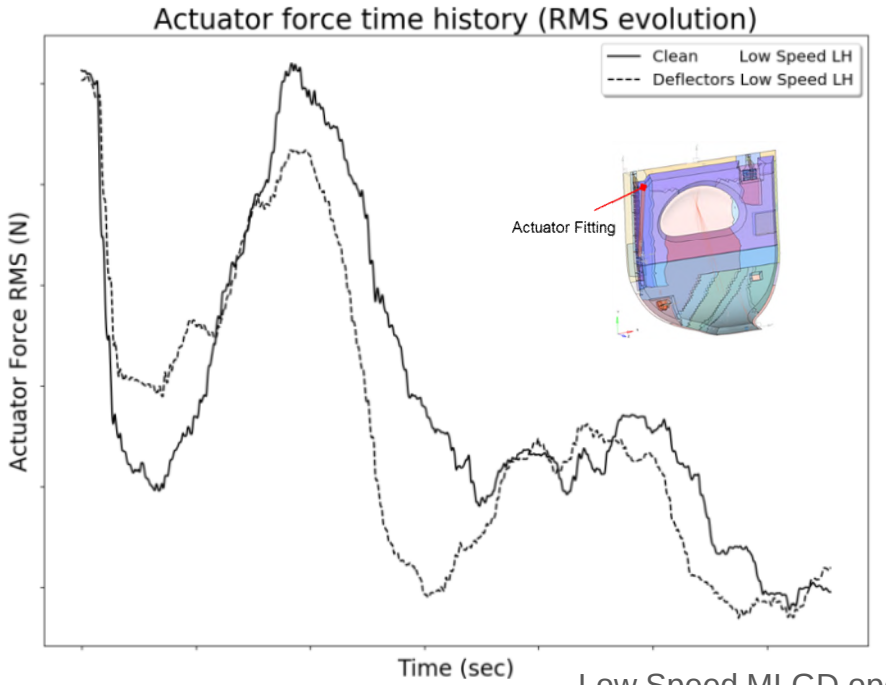

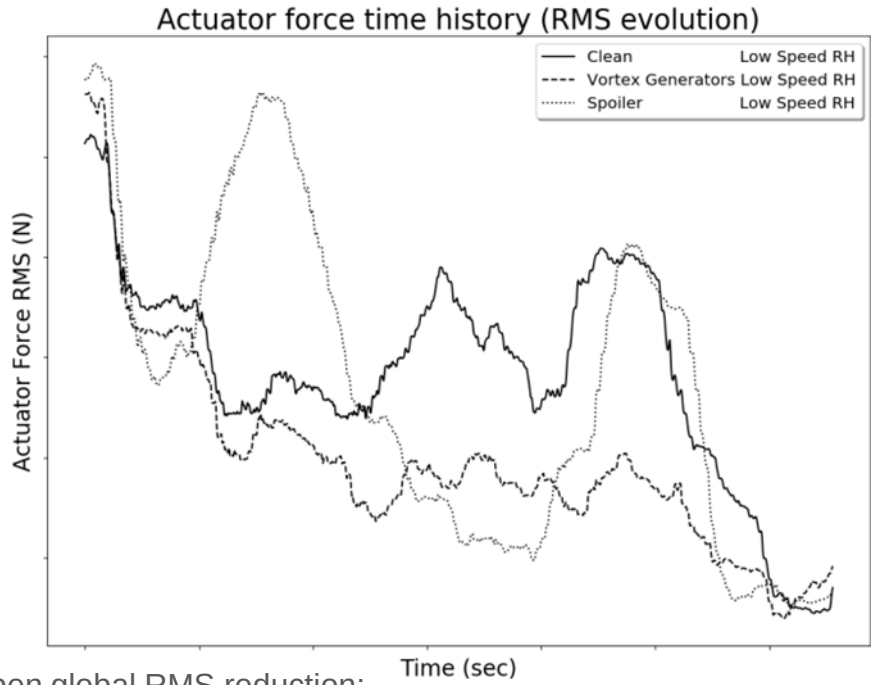

Low Speed MLGD open global RMS reduction:
Vortex Generators = 10.2%
Deflectors = 9.7%
Spoiler = 0.5%

Acceleration Reduction

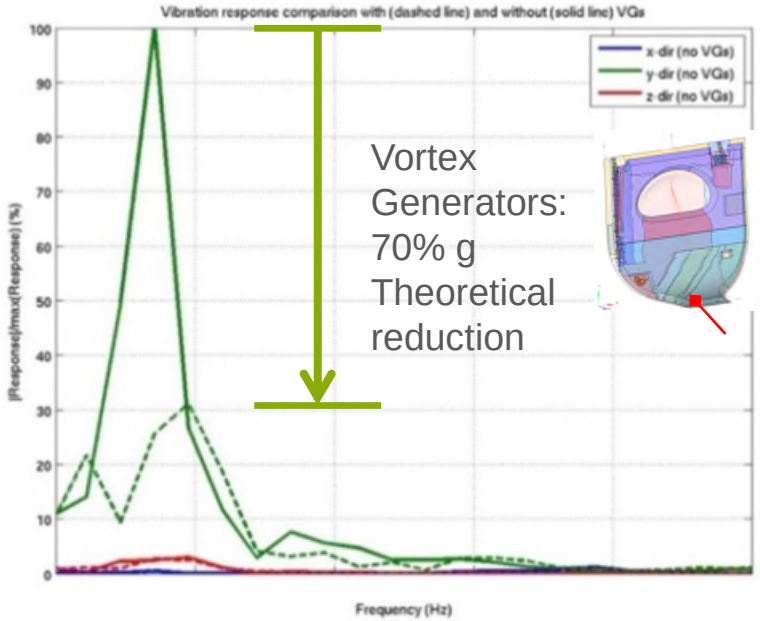

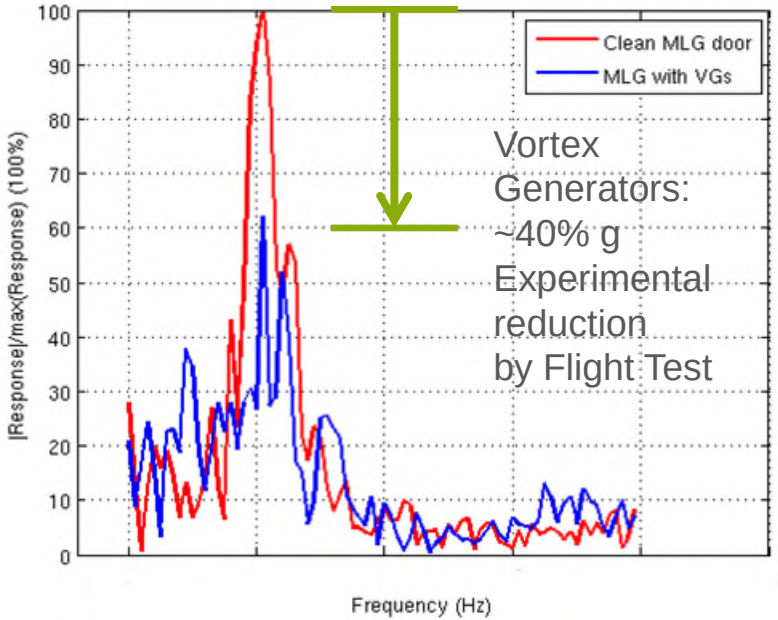

Conclusions

- **Extensive research** on the structural response of Main Landing Gear Doors under **operational conditions** of a typical **landing gear tricycle** configuration was presented and discussed.
- **Unsteady CFD computations** provided the root causes of aerodynamic excitation as the vortex shedding from the Nose Landing Gear and the flow separation on the Main landing gear doors.
- A **Ground Vibration Test** provided necessary information for the **update of the FEM** of the isolated door.
- **CFD-CSM Buffeting analyses** provided a good matching with flight test results:
  - Actuator force RMS with differences up to 2.4%.
  - Accelerations RMS with differences between 0.6 and 12% depending on sensor location. A poor model update of the 3rd mode caused higher discrepancies at the hinge line. Removing the 3rd mode from the modal base improved results.
- **Three different devices were designed, manufactured and flight-tested**, achieving the following reductions of the Main Landing Gear Door actuator RMS:
  - Vortex Generators up to 10.6%
  - Deflectors up to 12.5%
  - Spoilers between 0.5 and 11.2% depending on the speed

This project has received funding from the European Union's Seventh Framework Programme for research, technological development and demonstration under grant agreement No 604013, AFLONEXT project.